ISSN 1674-1056
http://cpb.iphy.ac.cn
http://iopscience.iop.org/cpb
中国物理 B
Chinese Physics
中国物理 Chinese Physics B

Spectral attenuation of a 400-nm laser pulse propagating through a plasma filament induced by an intense femtosecond laser pulse

Quan-Jun Wang(王全军)[1], Rao Chen(陈娆)[1], Jia-Chen Zhao(赵家琛)[1], Chun-Lin Sun(孙春霖)[2], Xiao-Zhen Wang(王小珍)[2], Jing-Jie Ding(丁晶洁)[1], Zuo-Ye Liu(刘作业)[1], Bi-Tao Hu(胡碧涛)[1]

Citation: Chin. Phys. B . 2020, 29(1): 013301 . **doi:** 10.1088/1674-1056/ab5a39
Journal homepage: http://cpb.iphy.ac.cn; http://iopscience.iop.org/cpb

What follows is a list of articles you may be interested in

Characterize and optimize the four-wave mixing in dual-interferometer coupled silicon microrings

Chao Wu(吴超), Yingwen Liu(刘英文), Xiaowen Gu(顾晓文), Shichuan Xue(薛诗川), Xinxin Yu(郁鑫鑫), Yuechan Kong(孔月婵), Xiaogang Qiang(强晓刚), Junjie Wu(吴俊杰), Zhihong Zhu(朱志宏), Ping Xu(徐平)
Chin. Phys. B . 2019, 28(10): 104211 . **doi:** 10.1088/1674-1056/ab3f9b

Energetic few-cycle pulse compression in gas-filled hollow core fiber with concentric phase mask

Yu Zhao(赵钰), Zhi-Yuan Huang(黄志远), Rui-Rui Zhao(赵睿睿), Ding Wang(王丁), Yu-Xin Leng(冷雨欣)
Chin. Phys. B . 2019, 28(6): 064207 . **doi:** 10.1088/1674-1056/28/6/064207

Analysis of third and one-third harmonic generation in lossy waveguides

Jianyu Zhang(张剑宇), Yunxu Sun(孙云旭), Qinghai Song(宋清海)
Chin. Phys. B . 2019, 28(6): 064206 . **doi:** 10.1088/1674-1056/28/6/064206

Experimental optimum design and luminescence properties of $NaY(Gd)(MoO_4)_2$: Er^{3+} phosphors

Jia-Shi Sun(孙佳石), Sai Xu(徐赛), Shu-Wei Li(李树伟), Lin-Lin Shi(石琳琳), Zi-Hui Zhai(翟梓会), Bao-Jiu Chen(陈宝玖)
Chin. Phys. B . 2016, 25(6): 063301 . **doi:** 10.1088/1674-1056/25/6/063301

Spectroscopic properties in Er Er^{3+}/Yb^{3+}Co-doped fluorophosphate glass

Zheng Tao,Qin Jie-Ming,Jiang Da-Yong,L&#; Jing-Wen,Xiao Sheng-Chun
Chin. Phys. B . 2012, 21(4): 043302 . **doi:** 10.1088/1674-1056/21/4/043302

Spectral attenuation of a 400-nm laser pulse propagating through a plasma filament induced by an intense femtosecond laser pulse*

Quan-Jun Wang(王全军)[1], Rao Chen(陈娆)[1], Jia-Chen Zhao(赵家琛)[1], Chun-Lin Sun(孙春霖)[2], Xiao-Zhen Wang(王小珍)[2], Jing-Jie Ding(丁晶洁)[1], Zuo-Ye Liu(刘作业)[1,†], and Bi-Tao Hu(胡碧涛)[1]

[1] *School of Nuclear Science and Technology, Lanzhou University, Lanzhou* 730000, *China*
[2] *College of Chemistry and Chemical Engineering, Lanzhou University, Lanzhou* 730000, *China*

(Received 5 August 2019; revised manuscript received 4 November 2019; accepted manuscript online 22 November 2019)

The spectral attenuation of a 400-nm probe laser propagating through a femtosecond plasma in air is studied. Defocusing effect of the low-density plasma is an obvious effect by examining the far-field patterns of the 400-nm pulse. Besides, the energy of 400-nm pulse drops after interaction with the plasma, which is found to be another effect leading to the attenuation. To reveal the physical origin behind the energy loss, we measure fluorescence emissions of the interaction area. The fluorescence is hardly detected with the weak 400-nm laser pulse, and the line spectra from the plasma filament induced by the 800-nm pump pulse are clearly shown. However, when the 400-nm pulse propagates through the plasma filament, the fluorescence at 391 nm from the first negative band system of N_2^+ is enhanced, while that from the second positive band of neutral N_2 at 337 nm remains constant. Efficient near-resonant absorption of the 400-nm pulse by the first negative band system occurs inside the plasma, which results in the enhanced fluorescence. Furthermore, the spectral attenuation of the 400-nm probe laser is measured as a function of the pump–probe time delay as well as the pump-pulse energy.

Keywords: defocusing effect, energy loss, enhanced fluorescence

PACS: 33.50.Dq, 42.65.–k, 42.68.Ca **DOI:** 10.1088/1674-1056/ab5a39

1. Introduction

An intense femtosecond laser pulse experiences a filamentation process when propagating in air. When the power exceeds a critical value P_{cr} (3 GW in air for the 800-nm Gaussian beam with pulse duration longer than 100 fs), the self-focusing induced by Kerr effect occurs and the laser intensity becomes higher and higher. The high intensity ionizes air molecules, resulting in the generation of a weak plasma. The plasma defocusing effect balances Kerr self-focusing and the intensity is clamped inside the plasma, creating a filament with a diameter around 100 μm.[1,2] Remarkably, it makes the laser filamentation fascinating that there are a lot of potential applications. It has been proposed to be used in many respects ranging from the remote sensing,[3–5] the triggering of lightning,[6] the detection of similar biological materials by filament-induced breakdown spectroscopy,[7] to the stand-off THz illumination,[8] and the generation of attosecond pulses.[9]

Many techniques were exploited to understand the laser filamentation process, which is pretty important for the further development of its potential applications. Among all these techniques, the measurement of the plasma fluorescence is an effective effort, which is employed to characterize the filament size and extract the electron density as well as electron temperature inside the filament.[10,11] Besides, electric cross-conductivity technique, the measurement of energy exchange between two femtosecond laser filaments and high harmonic generation were also proposed to acknowledge the laser filamentation.[12–14] Recently, unexpected lasing actions at 391 nm inside the plasma filament have been reported, appealing new techniques to further understand the dynamical process in both experiment and theory.[15–21] It is noticed that except amplification at 391 nm, other frequency components of the seeded pulses are weaker than its original spectra in the harmonic-seeded radiation-amplification experiment,[22] which is attributed to the defocusing effect induced by the plasma.

In this paper, we investigate the spectral attenuation of a 400-nm pulse with a high energy and a narrow spectral width induced by an 800-nm pump laser. The amplification at 391 nm is excluded as the spectra do not cover this region. Beside the plasma defocusing effect, the energy loss of the 400 nm pulse through near resonant absorption process is demonstrated as another effect that leads to the spectral attenuation by measuring the energy of 400-nm pulse and fluorescence emissions of the interaction area.

2. Experiment

The experiments are carried out using a Ti:sapphire laser system (Legend Elite-Duo, Coherent Inc.) as shown in Fig. 1.

*Project supported by the National Natural Science Foundation of China (Grant Nos. U1932133, 51733004, 51525303, and 21702085) and the Fundamental Research Funds for the Central Universities, China (Grant Nos. lzujbky-2016-35 and lzujbky-2018-it36).

†Corresponding author. E-mail: zyl@lzu.edu.cn

© 2020 Chinese Physical Society and IOP Publishing Ltd

The femtosecond laser pulse (1 kHz, 800 nm, ~ 120 fs, 5.8 mJ) from the Ti:sapphire laser with a beam radius of 5 mm is split into two arms (1 : 1) by a beam splitter. One beam serving as the pump pulse with energy up to 2.9 mJ is utilized to generate a plasma filament in air. The pump energy can be tuned by a continuously variable neutral density attenuator, which is set into the pump beam path right after the beam splitter. The other one is frequency doubled by a 0.2-mm thickness β-BBO crystal to produce the 400-nm pulse; it then serves as the probe pulse, whose energy is about 0.37 mJ. A high-resolution delay line with a minimum step of 0.52 fs allows us to scan the pump–probe time delay τ. The pump and the probe pulses are combined with a dichroic mirror (DM) and collinearly focused by a fused silica lens with focusing length of 150 mm. The spatial overlap of the pump and probe pulses is checked by a far-field measurement of the optical pattern, and the rough temporal superposition is examined by the defocusing pattern of the 400-nm pulse after passing though the plasma filament generated by the 800-nm pump pulse. Another BBO crystal is used to generate an SHG (sum frequency generation) for these two pulses to define the zero time between the pump and probe pulses. The zero time is chosen as the position where the SHG emission is the strongest by tuning the pump-pulse optical-path with the delay line. After the interaction, the collinear probe and pump pulses are focused again, and then reflected by several 400-nm high reflective mirrors. By this way, the pump and probe pulses are separated. The 400-nm pulse is coupled into a fiber-pigtailed spectrometer (Ocean Optics USB 4000) with a spectral resolution of 0.25 nm. A CCD camera is applied to measure the far-field pattern of the 400-nm pulse. The fluorescence of the plasma filament is also collected by a spherical mirror (SM) and then focused into the fiber-pigtailed spectrometer.

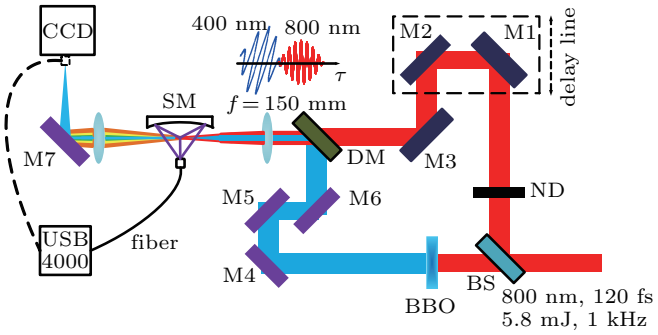


Fig. 1. The schematic diagram of the experimental setup for the measurement. M1, M2, M3: 800-nm high reflective mirrors; M4, M5, M6, M7: 400-nm high reflective mirrors. ND: the continuously variable neutral density attenuator. DM: the dichroic mirror. SM: the spherical mirror. USB 4000: the fiber-pigtailed spectrometer.

3. Results and discussion

The pump-pulse energy is first set to be 2.7 mJ to generate a plasma in air. The 400-nm pulse is then collinearly sent to interact with the plasma filament with a time delay. The spectra of the 400-nm pulse are attenuated, as illustrated by the black solid line in Fig. 2(a).

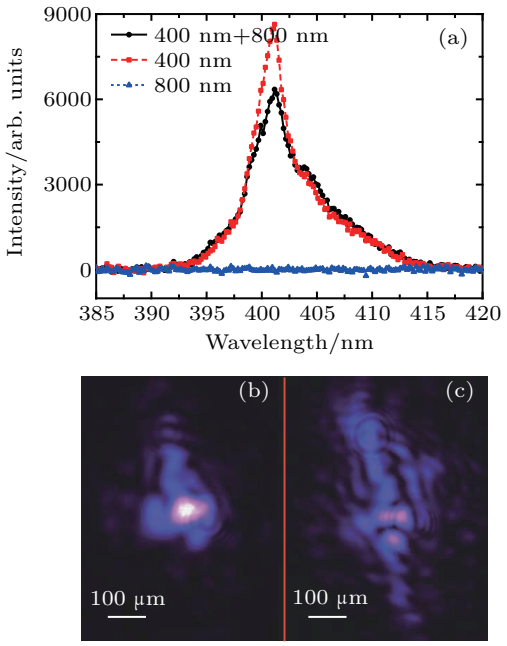


Fig. 1. (a) The spectra of the 400-nm pulse measured with (black circle) and without (red square) the plasma generated by the intense pump pulse with a pulse energy of 2.7 mJ. The spectrum of the pump pulse (blue triangle) is also shown to check the influence of the super continuum generation. The far-field pattern of the 400-nm pulse measured without (b) and with (c) the air plasma. The measurement is done at 3 mm in front of the focus to get a clear diverged pattern, and the pump–probe time delay is $\tau = 100$ fs.

The spectral intensity of the 400-nm pulse is about 70% of that measured without the presence of the plasma filament. The spectra of the plasma filament can be broadened to ultraviolet range due to the self-phase modulation effect, which is known as the super continuum generation. In order to check the influence of the continuum generation on the observed phenomenon, the spectra are measured without the 400-nm pulse, which is displayed by the blue dot line in Fig. 2(a). It turns to be zero in the measured range, excluding the effect on the spectrum measurement of the 400-nm pulse. Figure 2(c) demonstrates that the 400-nm pulse with a dark spot in the center of the far-field pattern has a larger area of intensity distribution compared to that without the plasma in Fig. 2(b). Then, the signal intensity is decreased in our measurement as a result of the divergence of 400-nm pulse. The pattern shown in Fig. 2(c) is caused by the defocusing effect of the low-density plasma, which have been explained in the time-resolved experiments.[23–25]

From the measurement above, we find that the defocusing effect of air plasma is a straight reason for the attenuation of the 400-nm pulse. Besides, the 400-nm pulse energy may drop with the pump pulse compared to that without the pump pulse, which can also lead to the reduced 400-nm signal. To verify this conjecture, we further measure the 400-nm pulse energy after the interaction with the pump pulse as a function of the pump–probe time delay. Figure 3(a) shows that the 400-nm

pulse energy drops rapidly from 0.367 mJ to 0.334 mJ during 250 fs. When the pump–probe time delay is at −130 fs, the head of the pump pulse just catches the tail of the 400-nm pulse. With time delay increasing, more parts of the 400-nm pulse overlap with the 800-nm pulse and lose more energy to the plasma. After 120 fs, these two pulses are separated and the 800-nm pulse now is in front of the 400-nm pulse. Based on the analysis above, the 400-nm pulse duration is estimated to be about 130 fs, as the pump pulse duration is clearly given (120 fs). We classify it as energy loss rather than energy exchange because there is no energy recovery when the pump–probe time delay is scanned from negative to positive, which is the most striking feature for energy exchange.[13] In fact, the energy loss lasts several picoseconds in our measurement.

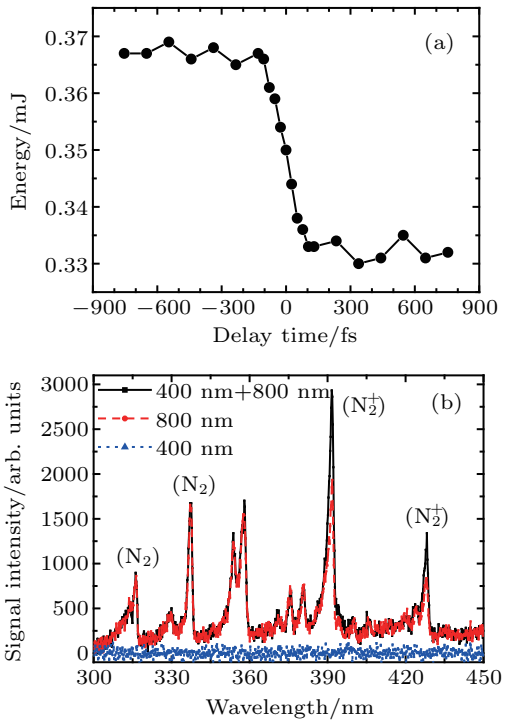


Fig. 3. (a) The dependence of the 400-nm pulse energy on the pump–probe time delay τ. Negative time delay means the 400-nm pulse is in front of the pump pulse. (b) Typical fluorescence spectra of the interaction area with the 400-nm pulse (blue dot line), plasma filament (red dash line), and both the 400-nm pulse and the plasma filament (black solid line). The energy of pump pulse is 2.7 mJ and the time delay τ is 200 fs.

In order to investigate the source of the energy loss, we measure the fluorescence signal of the interaction area, as displayed in Fig. 3(b). The fluorescence can not be detected with the 400-nm pulse alone, while that from the plasma filament induced by the 800-nm pump pulse is clearly shown. Surprisingly, the line spectrum of the first negative system of N_2^+ at 391 nm from the plasma filament induced by the 800-nm pump pulse is enhanced with the existence of the weak 400-nm pulse, whereas that from the excited nitrogen molecule $N_2(C^3\Pi_u)$ at 337 nm keeps constant. The undetected fluorescence with the 400-nm pulse and the unchanged fluorescence of 337 nm indicate that the weak 400-nm pulse could not ionize nitrogen molecules in air directly. Since the triplet state $N_2(C^3\Pi_u)$ is a spin forbidden process for direct high-field photonic excitation, two indirect excitation processes are proposed.[26,27] One is impact excitation channels from energetic electrons with the ground state nitrogen molecules, which is observed only with circularly polarized laser pulses.[27,28] The other is a dissociative recombination through the processes: $N_2^+ + 2N_2 \rightarrow N_4^+ + N_2$, $N_4^+ + e \rightarrow N_2(C^3\Pi_u) + N_2$, which is proportional to the population of N_2^+. Thus, the unchanged fluorescence signal from excited neutral molecules implies that the additional 400-nm pulse cannot change the population of the excited state $N_2(C^3\Pi_u)$, *i.e.*, the same ionization yield with or without the 400-nm pulse in our measurement. It suggests the function of the weak 400-nm pulse-repopulating the ion states of molecular nitrogen ions. There should be a strong coupling between these two states $N_2^+(X^2\Sigma_g^+, v = 0)$ and $N_2^+(B^2\Sigma_u^+, v' = 0)$ in one-photon, near-resonant laser condition. This strong coupling was verified in the Meinel band system of N_2^+, which was used to explain the population inversion between $N_2^+(B^2\Sigma_u^+, v' = 0)$ and $N_2^+(X^2\Sigma_g^+, v = 0)$.[17] In their review, near the peak of envelope of the 800-nm driver laser, the molecules were populated to the ground state of molecular nitrogen ions $N_2^+(X^2\Sigma_g^+)$ and excited states of molecular nitrogen ions $N_2^+(A^2\Pi_u)$ and $N_2^+(B^2\Sigma_u^+)$ by tunnel ionization. After the generation of molecular nitrogen ions, the residual of strong laser field induced a population transfer from $N_2^+(X^2\Sigma_g^+, v = 0)$ to $N_2^+(A^2\Pi_u, v' = 2)$. As the resonant wavelength between $N_2^+(X^2\Sigma_g^+, v = 0)$ and $N_2^+(A^2\Pi_u, v' = 2)$ is 787 nm,[29] the coupling is one-photon, near-resonant coherent excitation. Similarly, the 400-nm pulse efficiently excites the $N_2^+(X^2\Sigma_g^+, v = 0)$ to $N_2^+(B^2\Sigma_u^+, v' = 0)$ by a near-resonant absorption process, leading to the enhanced fluorescence of molecular nitrogen ions at 391 nm. The line spectrum at 428 nm, originated from the transition $N_2^+(B^2\Sigma_u^+, v' = 0) \rightarrow N_2^+(X^2\Sigma_g^+, v = 1)$, is enhanced as well.

The interaction between the two-level system of $N_2^+(X^2\Sigma_g^+,\ v = 0)$ and $N_2^+(B^2\Sigma_u^+,\ v' = 0)$ and the 400-nm pulse is given by the optical Bloch equation. The pulse width of 400-nm laser is around 130 fs, which is much shorter than the relaxation time of molecular nitrogen ions (nanosecond scale). Hence, the current case can be described by the equation without relaxation time

$$\partial\alpha/\partial t = -\Delta\beta, \tag{1a}$$

$$\partial\beta/\partial t = \Delta\alpha + \Omega\gamma, \tag{1b}$$

$$\partial\gamma/\partial t = -\Omega\beta, \tag{1c}$$

where α and β describe dispersion and absorption of electric dipole moment; γ denotes the population probability dif-

ference between $N_2^+(B^2\Sigma_u^+, v'=0)$ and $N_2^+(X^2\Sigma_g^+, v=0)$. $\Delta = \omega_{BX} - \omega$; ω_{BX} and ω represent the angular frequency of the transition from $N_2^+(B^2\Sigma_u^+, v'=0)$ to $N_2^+(X^2\Sigma_g^+, v=0)$ at 391 nm and the angular frequency of 400-nm pulse, respectively. $\Omega = (\mu/\hbar)\sqrt{(8\pi\varepsilon_0/c)I_0(t)}$ is Rabi frequency with μ, $\hbar$, ε_0, c, and $I_0(t)$ denoting the electronic transition moment, the reduced Planck constant, the vacuum permittivity, the light speed, and the envelope of laser intensity, respectively. In this ultrafast process, $I_0(t)$ can be replaced by the laser peak intensity, *i.e.*, 9×10^{12} W·cm^{-2}. Before the interaction between the two-level system and 400-nm pulse, the initial α and β are zero. We assume that 10% molecular nitrogen ions populate in the $N_2^+(B^2\Sigma_u^+, v'=0)$ state and 90% populate in the $N_2^+(X^2\Sigma_g^+, v=0)$ state.[17] With the effective electronic transition moment of 1.078 Debye,[30] the population probability difference γ is shown in Fig. 4. In the 400-nm laser field, γ experiences strong oscillations, demonstrating the near-resonant, one-photon coupling above. Efficient population transfer takes place between the ground and the excited electronic state. At the end of the laser pulse, the populations in the $N_2^+(B^2\Sigma_u^+, v'=0)$ increase significantly, while those in the $N_2^+(X^2\Sigma_g^+, v=0)$ decrease, explaining the phenomenon of enhanced fluorescence of molecular nitrogen ions. In the same time, the unchanged fluorescence signal of nitrogen molecules manifests that there is no selectivity of N_2^+ in reactions $N_2^+ + N_2 \rightarrow N_4^+$; $N_4^+ + e \rightarrow N_2(C^3\Pi_u) + N_2$, populating the excited electronic state of nitrogen molecules.

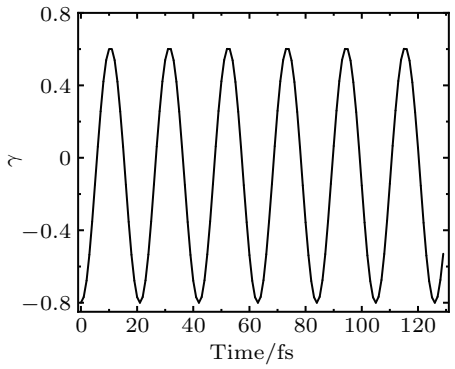


Fig. 4. The temporal evolution of the population probability difference in the 400nm laser field with an intensity of 9×10^{12} W·cm^{-2}.

To gain a deeper insight, we define a signal I/I_0 as the spectral intensity of the 400-nm pulse measured with the presence of the plasma filament divided by that measured without the plasma filament. Results in Fig. 5(a) show the signal I/I_0 as a function of the pump–probe time delay τ in the range from −0.5 ps to 5.0 ps. The signal I/I_0 first decreases rapidly to 0.58 on the time scale of 250 fs, and then increases to 0.8 right after the separation of the two pulses. Afterwards, it experiences a slow rise in the following several picoseconds. To understand the significant drop at time delay of zero, the enhanced ratio γ which is defined as the intensity of plasma fluorescence at 391 nm with the 400-nm pulse divided by that without the 400-nm pulse is displayed in Fig. 5(a) as a function of time delay. A remarkable increase can be observed at the delay time of $\tau = 0$, demonstrating an enhancement of the ionization of N_2^+,[26] *i.e.*, the increase of the electron density. The defocusing effect intensifies and a deeper near-resonant absorption happens, causing the significant drop of the signal at time delay of zero.

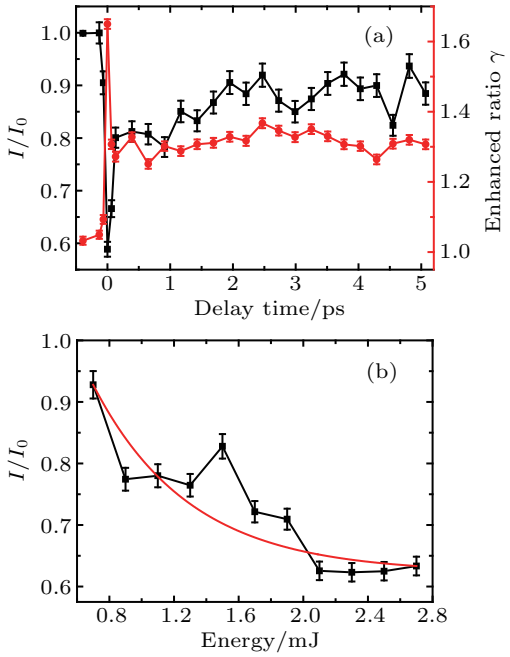


Fig. 5. (a) The signal I/I_0 (black square) of the probe pulse and the enhanced ratio γ (blue circle) as a function of the pump–probe time delay with a pump-pulse energy of 2.7 mJ. (b) The dependence of I/I_0 on the pump-pulse energy with a fixed pump–probe time delay of 50 fs.

Figure 5(b) displays the signal I/I_0 with the incident pump-pulse energy varying from 0.7 mJ to 2.7 mJ. With a pump-pulse energy of 0.7 mJ, the plasma density is relative low and the attenuation effect is pretty weak. With the increase of the pump-pulse energy, the laser intensity in the plasma filament rises until the clamped intensity, and the plasma density increases dramatically as the plasma is generated through the highly nonlinear multiphoton/tunnel ionization process.[2] In addition, the plasma length also increases slightly with the pump-pulse energy, despite the application of the short focus lens in the measurement.[31] Both of them give rise to the more intense spectral attenuation of the 400-nm pulse. The laser intensity inside the plasma will be clamped to a certain value, and it will keep constant with further increase of the incident pump-pulse energy. The extra energy flows into energy reservoir rather than strengthen the plasma density in filament, *i.e.*, the plasma density is saturated. With an incident pump-pulse energy of 2.1 mJ in our case, the laser intensity reaches its

clamped value. The attenuated signal tends to be constant when the pump pulse energy exceeds 2.1 mJ. The red fitting curve in Fig. 5(b) is utilized to describe the trend of the signal I/I_0 when the pump energy is tuned in the measurement range.

4. Conclusion

In summary, we investigated the spectral attenuation of the 400-nm pulse caused by the plasma filament in air. To unveil the physics behind the observed phenomenon, we observed the far-field pattern of the 400-nm pulse, measured the energy loss of the 400-nm pulse and recorded the fluorescence emissions of the interaction area. It is believed that the defocusing effect of the low-density plasma and energy loss jointly result in the spectral attenuation. The energy loss process is induced by the near-resonant absorption, and efficient population transfer occurs in nitrogen molecular ions between the ground and excited states. The present study reveals the interplay between the 400-nm pulse and the plasma filament, which will benefit the implications for investigating the excited-state dynamics of molecular ions in intense laser fields.

Acknowledgement

We thank Shaohua Sun for insightful discussions.

References

[1] Couairon A and Mysyrowicz A 2007 *Phys. Rep.* **441** 47
[2] Chin S L 2010 *Femtosecond laser filamentation*, Vol. 55 (New York: Springer) pp. 1–55
[3] Kasparian J, Rodríguez M, Méjean G, Yu J, Salmon E, Wille H, Bourayou R, Frey S, André Y B, Mysyrowicz A, Sauerbrey R, Wolf J P and Wöste L 2003 *Science* **301** 61
[4] Liu J, Dai J, Chin S L and Zhang X C 2010 *Nat. Photon.* **4** 627
[5] Yuan S, Chin S L and Zeng H 2015 *Chin. Phys. B* **24** 014208
[6] Miki M and Wada A 1996 *J. Appl. Phys.* **80** 3208
[7] Xu H, Méjean G, Liu W, Kamali Y, Daigle J F, Azarm A, Simard P, Mathieu P, Roy G, Simard J R and Chin S L 2007 *Appl. Phys. B* **87** 151
[8] Liu Y, Houard A, Prade B, Akturk S, Mysyrowicz A and Tikhonchuk V 2007 *Phys. Rev. Lett.* **99** 135002
[9] Sansone G, Benedetti E, Calegari F, Vozzi C, Avaldi L, Flammini R, Poletto L, Villoresi P, Altucci C, Velotta R, Stagira S, De Silvestri S amd Nisoli M 2006 *Science* **314** 443
[10] Filin A, Compton R, Romanov D and Levis R 2009 *Phys. Rev. Lett.* **102** 155004
[11] Shi L, Li W, Wang Y, Lu X and Zeng H 2011 *Phys. Rev. Lett.* **107** 095004
[12] Tzortzakis S, Prade B, Franco M and Mysyrowicz A 2000 *Opt. Commun.* **181** 123
[13] Liu Y, Durand M, Chen S, A. Houard, Prade B, Forestier B and Mysyrowicz A 2010 *Phys. Rev. Lett.* **105** 055003
[14] Ding J, Ding P, Liu Z and Hu B 2016 *Sci. China- Phys. Mech. Astron.* **59** 633001
[15] Chin S L and Xu H 2015 *Chin. Phys. B* **24** 013301
[16] Xu H, Lötstedt E, Iwasaki A and Yamanouchi K 2015 *Nat. Commun.* **6** 8347
[17] Yao J, Jiang S, Chu W, Zeng B, Wu C, Lu R, Li Z, Xie H, Li G, Yu C, Wang Z, Jiang H, Gong Q and Cheng Y 2016 *Phys. Rev. Lett.* **116** 143007
[18] Lei M, Wu C, Zhang A, Gong Q and Jiang H 2017 *Opt. Express* **25** 4535
[19] Liu Y, Ding P, Ibrakovic N, Bengtsson S, Chen S, Danylo R, Simpson E R, Larsen E W, Zhang X, Fan Z, Houard A, Mauritsson J, L'Huillier A, Arnold C L, Zhuang S, Tikhonchuk V and Mysyrowicz A 2017 *Phys. Rev. Lett.* **119** 203205
[20] Zhong X, Miao Z, Zhang L, Liang Q, Lei M, Jiang H, Liu Y, Gong Q and Wu C 2017 *Phys. Rev. A* **96** 043422
[21] Liu Z, Yao J, Chen J, Xu B, Chu W and Cheng Y 2018 *Phys. Rev. Lett.* **120** 083205
[22] Ni J, Chu W, Jing C, Zhang H, Zeng B, Yao J, Li G, Xie H, Zhang C, Xu H, Chin S L, Cheng Y and Xu Z 2013 *Opt. Express* **21** 8746
[23] Azarm A, Ramakrishna S, Talebpour A, Hosseini S, Teranishi Y, Xu H, Kamali Y, Bernhardt J, Lin S, Seideman T and Chin S L 2010 *J. Phys. B: At. Mol. Opt. Phys.* **43** 235602
[24] Liu J, Duan Z, Zeng Z, Xie X, Deng Y, Li R, Xu Z and Chin S L 2005 *Phys. Rev. E* **72** 026412
[25] Théberge F, Liu W, Simard P T, Becker A and Chin S L 2006 *Phys. Rev. E* **74** 036406
[26] Xu H, Azarm H, Bernhardt J, Kamali Y and Chin S L 2009 *Chem. Phys.* **360** 171
[27] Mitryukovskiy S, Liu Y, Ding P, Houard A, Couairon A and Mysyrowicz A 2015 *Phys. Rev. Lett.* **114** 063003
[28] Wang Q, Zhang Y, Wang Z, Ding J, Liu Z and Hu B 2016 *Chin. Opt. Lett.* **14** 110201
[29] Lofthus A and Krupenie P H 1977 *J. Phys. Chem. Ref. Data* **6** 113
[30] Langho S R and Bauschlicher C W Jr 1988 *J. Chem. Phys.* **88** 329
[31] Luo Q, Liu W and Chin S L 2003 *Appl. Phys. B* **76** 337